



ChemComm

Self-assembling materials functionalizing bio-interfaces of phospholipid membranes and extracellular matrices

Journal:	<i>ChemComm</i>
Manuscript ID	CC-FEA-04-2023-001875.R1
Article Type:	Feature Article

SCHOLARONE™
Manuscripts

ARTICLE

Self-assembling materials functionalizing bio-interfaces of phospholipid membranes and extracellular matrices

Received 00th January 20xx,
Accepted 00th January 20xx

Noriyuki Uchida,^a Takahiro Muraoka^{*a,b,c}

DOI: 10.1039/x0xx00000x

This Feature Article focuses on recent studies on the development of self-assembling materials that mimic and control dynamic bio-interfaces. Extracellular matrix (ECM) is a fundamental tissue at the cellular interface constructed by networks of fibrous proteins, which regulates a variety of cellular activities. Reconstruction of ECM has been demonstrated by self-assembling peptides. By combining the dynamic properties of the self-assembling peptides conjugated with full-length proteins, peptide-based supramolecular materials enable neuronal migration and regeneration of injured neural tissue. The phospholipid bilayer is the main component of the cell membrane. The morphology and deformation of the phospholipid bilayer relate directly to dynamic interfacial functions. Stabilization of the phospholipid nanosheet structure has been demonstrated by self-assembling peptides, and the stabilized bicelle is functional for extended blood circulation. By using a photo-responsive synthetic surfactant showing a mechanical opening/closing motion, endocytosis-like outside-in membrane deformation is triggered. The outside-in deformation allows for efficient encapsulation of micrometer-size substances such as phage viruses into the liposomes, and the encapsulated viruses can be delivered to multiple organs in a living body via blood administration. These supramolecular approaches to mimicking and controlling bio-interfaces present powerful ways to develop unprecedented regenerative medicines and drug delivery systems.

Introduction

Various cellular functions occur through the dynamic actions of biomacromolecules and supramolecular assemblies located at bio-interfaces (Fig. 1a). Typical dynamic functions of the bio-interfaces

in cellular activities include adhesion, signal transduction, and substance transportation. Extracellular matrix (ECM), a complex network of proteins and other biomolecules, is one such bio-interface.^{1,2} ECM adheres to membrane protein receptors such as cadherin via ligands of the ECM and regulates dynamic cellular functions such as migration. ECM also shows a release of signaling factors to trigger cell differentiation. For example, secreted proteins belonging to the hedgehog family interact with and dissociate from heparan sulfate proteoglycans generating the morphogen gradient essential for development.^{3,4} Another important architectural component of the bio-interface is phospholipid bilayers. The phospholipid bilayers are the major component of cellular and

^a Department of Applied Chemistry, Graduate School of Engineering, Tokyo University of Agriculture and Technology, 2-24-16 Naka-cho, Koganei, Tokyo 184-8588, Japan

^b Institute of Global Innovation Research, Tokyo University of Agriculture and Technology, 3-8-1 Harumi-cho, Fuchu-shi, Tokyo 183-8538, Japan

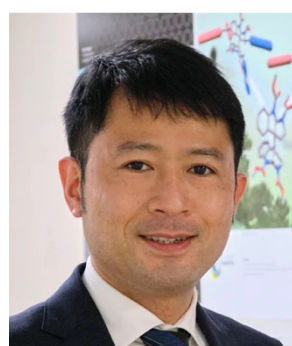
^c Kanagawa Institute of Industrial Science and Technology (KISTEC), 705-1 Shimoimaizumi, Ebina, Kanagawa 243-0435, Japan



Noriyuki Uchida

Noriyuki Uchida studied chemistry at Keio University for his B.Sc. and obtained a Ph.D. from The University of Tokyo in 2015 in the group of Prof. Aida. After a postdoctoral stay at RIKEN, he was appointed as an assistant professor at Tokyo University of Agriculture and Technology.

His current work is focused on supramolecular materials using biomacromolecules.



Takahiro Muraoka

Takahiro Muraoka studied chemistry and biotechnology at The University of Tokyo where he obtained a Ph.D. in 2007 in the group of Prof. Aida. After postdoctoral training at Northwestern University, he worked as an assistant professor in Tohoku University (2008–2015) and Tokyo Institute of Technology (2015–2017).

He is now a professor at Tokyo University of Agriculture and Technology. His work is focused on biomimetic materials using synthetic molecules, such as artificial extracellular matrices and membrane-deforming materials.

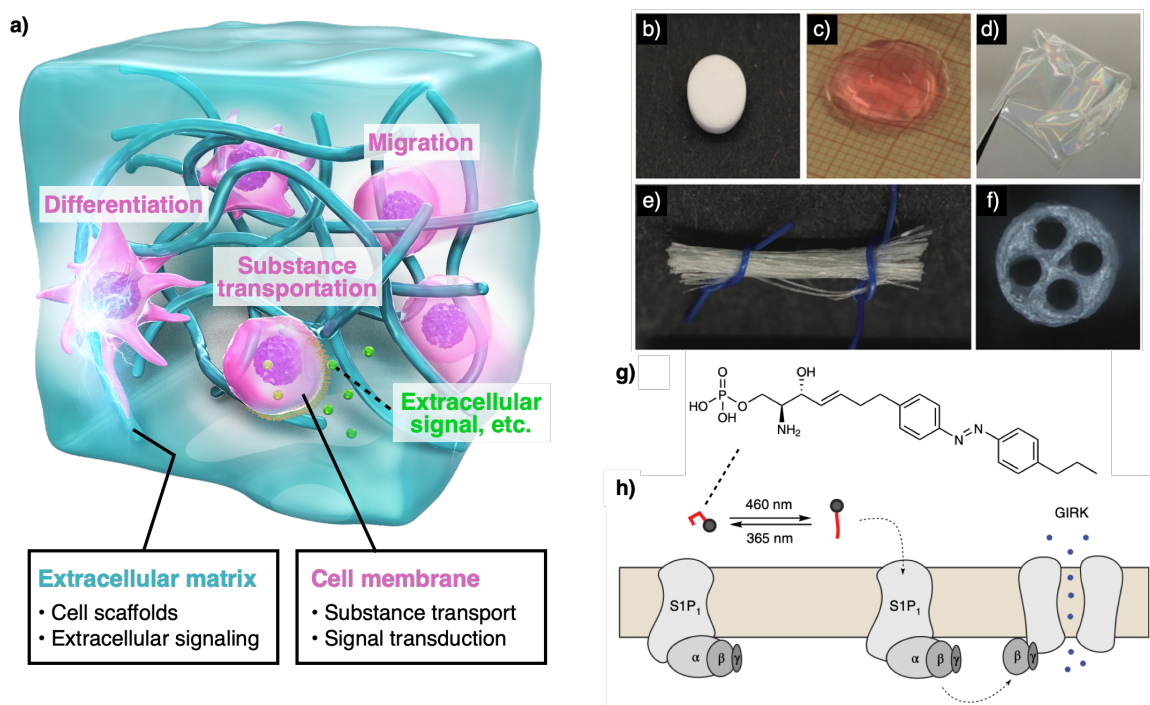


Fig. 1 (a) Diagram showing the interfaces in cellular activity and their functions. The extracellular matrix forming the interface between cells in a tissue that is involved in the differentiation and migration of cells. The cellular membrane forming the interface between the intracellular and extracellular environments is involved in substance transportation and signal transduction. Photographs of (b) freeze-dried collagen type I sponge, (c) collagen type II hydrogel loaded with cells, (d) transparent collagen type I film, (e) a bundle of extruded collagen type I fibers, and (f) multichannel collagen type I neural conduit as examples of artificial extracellular matrices.⁸ (g) Chemical structure of an azobenzene-containing artificial phospholipid and (h) schematic representation of photo-control of membrane channel as an example of an artificial cellular membrane.²⁷ Reproduced from reference 8 with permission from Wiley, copyright 2019, and reference 27 with permission from Nature Publishing Group, copyright 2019.

organelle membranes and contribute to fundamental cellular activities,^{5–7} such as substance transportation and intracellular signal transduction. Stimuli-responsive transformation is a notable characteristic function of the phospholipid bilayers for transportation. The deformation of the membranes regulates substance transportation in both directions, *i.e.*, exocytosis, as the transportation from the intracellular to the extracellular environment, and endocytosis, as the uptake of substances from the extracellular to the intracellular environment. The two-dimensional architecture of the phospholipid bilayers also provides media for embedding proteins. The membrane-embedded proteins are the central molecules performing membrane-mediated signal transduction by sensing external signals to regulate cell growth and differentiation. Recent progress in supramolecular chemistry and nanotechnology has made it possible to create materials that functionalize and control bio-interfaces by mimicking the ECM and membrane proteins. One important category of material for constructing artificial ECM is biological polymers, such as collagens (Fig. 1b–f)^{8,9} and silk^{10,11}, applicable to cell culturing as scaffold materials. Self-assembling peptides are another class of biomaterials for developing ECM-mimetics with several important advantages, such as the possibility of tailoring the properties by

modifying the amino acid sequences, the capability to form three-dimensional networks affording hydrogels, and high biocompatibility.^{12–23} By incorporating bioactive motifs such as RGD, the functionalities of the self-assembling peptides can be tuned and expanded to show cell adhesive properties.^{24–26} For functionalizing the membranes with transportation capabilities, synthetic membrane channels have been extensively developed. The synthetic channels allow for the transportation of ions and small molecules with selectivity and stimuli-responses functioning not only in the artificial bilayers but also in cellular membranes (Fig 1g, h).^{27,28} The cell periphery is highly dynamic showing a release of growth factors from the ECM, binding with the receptors at the cell surface, and incorporation of molecules, macromolecules, and even molecular assemblies such as viruses into cells by membrane deformation. Such dynamic molecular actions at the bio-interfaces constitute the signaling processes that trigger numerous cell activities such as differentiation and proliferation. Based on the dynamic activities seen in the cell periphery, a materials design including signal releasing and incorporation functionalities should be effective for advancing the technologies of cellular regulation and tissue engineering. In this Feature Article, recent studies on the development of self-assembling materials functionalizing the bio-

interfaces are highlighted. Self-assembling peptides as artificial ECMs capable of immobilizing cell-adhesion proteins and releasing growth factors allow for neural tissue regeneration. Synthetic lipids with photochemical responses trigger membrane deformation, which is useful for transportation, protection, and *in vivo* delivery of phages.

Stiffness-controlled supramolecular peptide hydrogels as artificial extracellular matrices for enhanced neuronal migration

Among self-assembling peptides, peptide amphiphiles bearing fatty acid chains at a terminus of the peptide main chain are known to construct nanofibres by forming cylindrical micelles.^{12–14} Diphenylalanine has also been extensively studied as a backbone to afford supramolecular fibres.^{15,16} Such supramolecular peptide fibres provide three-dimensional networks with a gelation capability as ideal scaffold materials for mimicking and controlling the bio-interface between cells due to their advantages such as easy preparation, surface tunability, and biocompatibility. Among them, peptides consisting of repeating sequences of RADA (Arg-Ala-Asp-Ala) such as RADA16¹⁹ are also known to form supramolecular nanofibres in aqueous media through β -sheet-type hydrogen

bonding and hydrophobic interaction corresponding to the alternating sequence of hydrophilic and hydrophobic amino acid residues. Since RADA-based peptides are composed of naturally occurring amino acids, they can also be used as a tag sequence incorporated into proteins of interest with an *E. coli* expression system for binding with the supramolecular nanofibres. In addition, peptide fibres that exhibit various dynamic behaviours can be designed by tuning the amino acid sequences, particularly in the hydrophobic part.^{20–23} For example, it has been reported that the conformational flexibility of peptide fibres can be a critical factor in controlling the stiffness of the hydrogels made of the entangled supramolecular nanofibres. Introducing glycine residues generally enhances the conformational flexibility of polypeptide chains. Despite the enhanced flexibility, A8G (Fig. 2a), a mutant of RADA16 in which the alanine in the middle of the peptide sequence is replaced with glycine, forms bundled nanofibres and a more robust hydrogel than RADA16 (Fig. 2b, c, and e).²⁰ On the other hand, A16G (Fig. 2a), in which the terminal alanine residue of RADA16 is replaced with glycine, forms curved fibres seen on transmission electron microscopy (TEM) (Fig. 2d). Molecular dynamics (MD) simulations also visualized similar self-assembling morphology (Fig. 2f). The hydrogel made of A16G showed lower stiffness than that of RADA16, suggesting that the morphological differences of the fibres could affect the macroscopic properties.

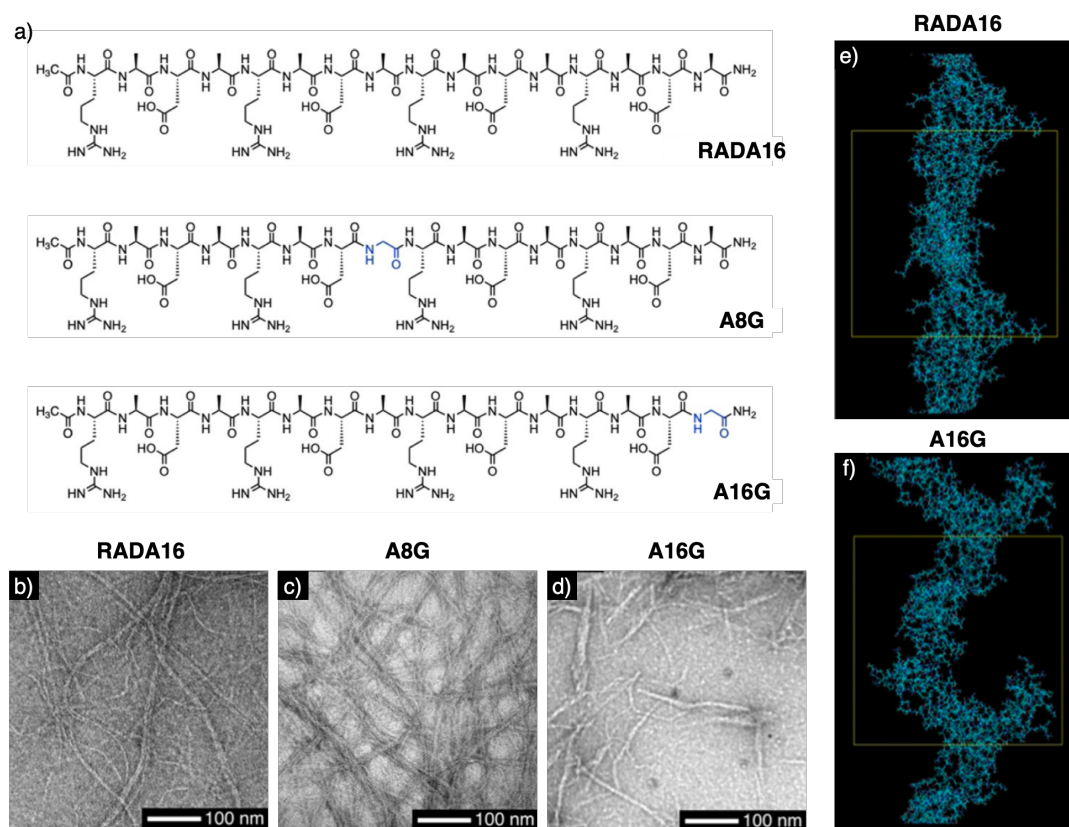


Fig. 2 (a) Molecular structures of RADA16, A8G, and A16G. Glycine residues are highlighted in blue. Transmission electron microscopic (TEM) image of (b) RADA16, (c) A8G, and (d) A16G. Snapshots of supramolecular structures of (e) RADA16 and (f) A16G in water at 300 K calculated by all-atom molecular dynamics simulations. Yellow rectangles represent the unit cells.²⁰ Reproduced from reference 20 with permission from Wiley, copyright 2019.

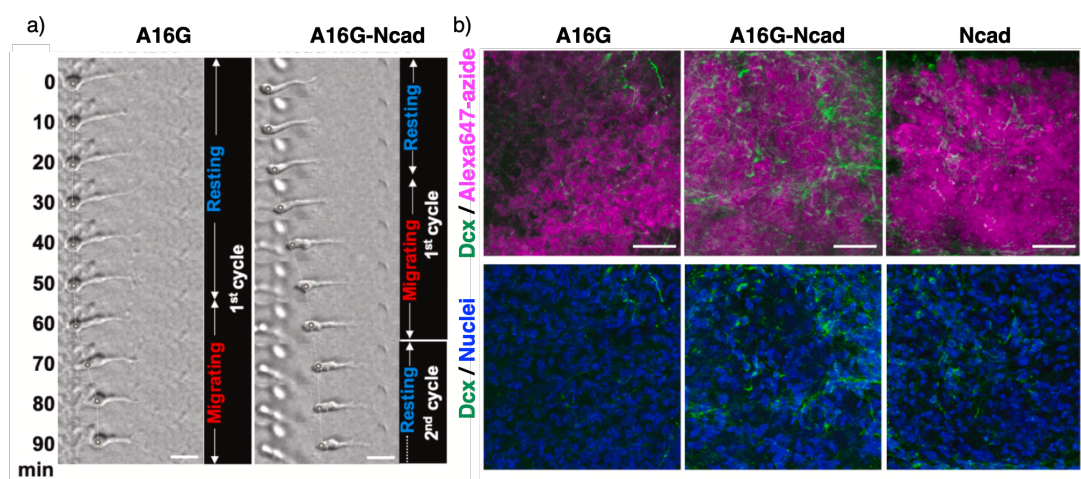


Fig. 3 (a) Migration profiles of neuroblasts in contact with the biomaterials. Light microscopy images of neuroblasts migrating on an A16G or A16G-Ncad hydrogel-coated dish at different time-points. Scale bars: 10 μm . (b) Distribution of neuroblasts in hydrogels formed in the injured neocortex. Z-stack projection image of Dcx+ neuroblasts (green) distributed inside the A16G hydrogel, a mixture of A16G and A16G-Ncad hydrogel or an A16G hydrogel mixed with Ncad-Fc (Ncad hydrogel) four days after injection. The hydrogels are visualized with Alexa647-conjugated azide (Alexa647-azide, magenta). Scale bars: 50 μm .²¹ Reproduced from reference 21 with permission from Elsevier, copyright 2023.

The enhanced mobility, decreased stiffness, and thixotropic property of A16G hydrogel can be advantageous for injection in biomedical applications. The mammalian brain has a very limited capability for regeneration of lost neurons and regaining function after injury.^{29–36} Promoting the migration of young neurons derived from endogenous neural stem cells (neuroblasts) using biomaterials is a promising new approach to help the brain recover after injury. However, delivering sufficient neuroblasts to distant injury sites has been a critical challenge^{37–40} due to the limited number of scaffold cells for inducing neuroblast migration. It has been shown that hydrogels consisting of A16G and A16G-tagged N-cadherin (A16G-Ncad) can address the above issue.²¹ N-cadherin plays an important role in the migration of neuroblasts along radial glial fibres in the injured neonatal neocortex.⁴¹ Time-lapse imaging of ventricular-subventricular zone neuroblasts on culture dishes coated with A16G or a mixture of A16G and A16G-Ncad hydrogels showed that the migration rate of neuroblasts was significantly higher on the hydrogel containing A16G-Ncad than on A16G alone (Fig. 3a). When the neonatal neocortex is injured at low temperature, and, subsequently, hydrogels composed of A16G, a mixture of A16G and A16G-Ncad or a mixture of A16G and Ncad are injected at the site of injury, Dcx+ (a marker for neuroblasts) is abundantly observed in the hydrogel of the mixture of A16G and A16G-Ncad. In contrast, neuroblasts are seen sparsely in the hydrogels made of A16G alone and a mixture of A16G and Ncad (Fig. 3b), indicating that A16G hydrogel containing A16G-Ncad efficiently facilitates the migration of neuroblasts into the injured neocortex *in vivo*. This study demonstrates that fibrous self-assembly of A16G peptide and A16G-Ncad mimics both the structure and dynamic function of intrinsic scaffold cells, providing a novel strategy for neuro-regenerative therapy.

Peptide fibres capable of efficient incorporation and release of growth factors for neural tissue regeneration

Proteins secreted from cells are efficiently bound to and released from ECMs during injured tissue regeneration if the ECMs remain intact after injury. For example, the peptide domains of placenta growth factor-2 and laminin α subunit have high affinity to ECMs and induce signal transduction from their receptors, enhancing tissue repair.^{42,43} However, after severe tissue injury, a secreted protein needs to be provided along with the ECMs. Here, incorporating and releasing secreted proteins are generally incompatible, and thus the development of peptide-based materials capable of incorporating and releasing secreted proteins has been challenging. Cell-adhesive fibre-forming peptides with jigsaw-shaped hydrophobic surfaces (JigSAP)²² can be used for efficient incorporation and sustained release of proteins. JigSAP incorporating JigSAP-tagged vascular endothelial growth factor (VEGF)^{44,45} shows regenerative therapeutic effects in stroke models without cell transplantation. AXXXA and GXXXG amino acid sequences are structural motifs found in glycoprotein A.^{46,47} These motifs show α -helix-to- β -strand conformational transitions, generating a jigsaw-shaped hydrophobic surface that dimerizes with dovetail packing. This characteristic hydrophobic dimerization prompts nanofibre formation through β -sheet assembly. JigSAP, consisting of Ac-RIDARMRADIR-NH₂ sequence, possesses the AXXXA motif in the hydrophobic part and shows one-dimensional self-assembly in aqueous media *in silico* calculated by MD simulation (Fig. 4a and b). When JigSAP (1 wt%) is dispersed in Dulbecco's modified Eagle's medium (DMEM), circular dichroism (CD) spectroscopic analysis visualizes a conformational change from helical or coil forms to β -sheet over 100 hours. In the

transition to β -sheet, JigSAP forms nanofibres with an average width of 3.2 nm and length of several μm (Fig. 4c), and the dispersion becomes a hydrogel (Fig. 4d). Interestingly, the JigSAP hydrogel exhibits a remarkably high rigidity (1.1×10^4 Pa), and the storage modulus G' and loss modulus G'' of the JigSAP hydrogel monotonically decrease with increasing shear strain in the rheological analysis. The monotonic decrease of G'' results in a strain thinning profile that is typically observed in covalently polymerized materials; therefore, this shows that supramolecular nanofibres of JigSAP are robust. When full-length enhanced green fluorescent protein (EGFP) is covalently conjugated with JigSAP (EGFP-JigSAP), 5V (EGFP-5V), and RADA16 (EGFP-RADA16) at the C-terminus, there is a dramatic difference in incorporation efficiency between JigSAP-tagged and non-tagged EGFP proteins; EGFP-JigSAP is incorporated at 93 mol%, whereas non-tagged EGFP is incorporated at only 3 mol%. Similarly, EGFP proteins tagged with 5V and RADA16 show higher incorporation efficiency into the corresponding peptide nanofibres than untagged EGFP (Fig. 4i and j, EGFP-5V: 66 mol%, EGFP-RADA16: 55 mol%). Importantly, the JigSAP hydrogel shows more efficient long-term

release of the incorporated peptide-tagged proteins than the hydrogels consisting of other self-assembling peptides. The protein release profile from the gel shows that 21 mol% of EGFP-JigSAP incorporated into the JigSAP nanofibres is released after 24-hour incubation at 37 $^{\circ}\text{C}$, and the percentage of released protein increases to 39 mol% after 168 hours of incubation (Fig. 4k). In contrast, the release of EGFP-5V and EGFP-RADA16 stagnates after 48 hours of incubation, and only 5 mol% and 8 mol%, respectively, are released even after 168 hours (Fig. 4k). JigSAP capable of the efficient release of full-length proteins can be used for neuronal regeneration (Fig. 4e). When phosphate-buffered saline (PBS) (Fig. 4f and k), 1.0 wt% JigSAP (Fig. 4g and l), VEGF-bound JigSAP (Fig. 4h and m), 1.0 wt% JigSAP and 1.6 ng of non-tagged VEGF (VEGF + JigSAP; Fig. 4i and n), or 1.0 wt% JigSAP incorporating 1.6 ng of VEGF-bound JigSAP (VEGF-JigSAP + JigSAP; Fig. 4j and o) are injected into the injured cortex of a mouse model of ischaemic stroke produced by distal middle cerebral artery occlusion, the number of double-positive cells with laminin, an endothelial cell marker, and a thymidine analogue (EdU), increases

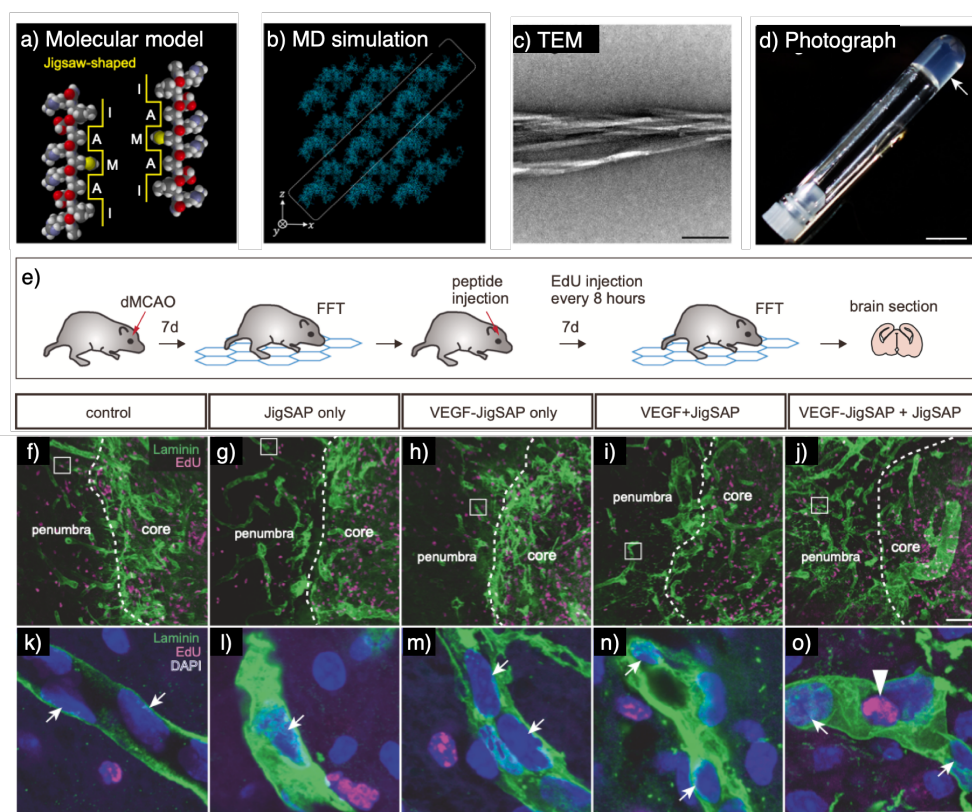


Fig. 4 (a) Space-filling models of Ac-RIDARMRADIR-NH₂ (JigSAP), showing the jigsaw-shaped hydrophobic surfaces. (b) A snapshot of supramolecular structures of JigSAP in water at 310 K obtained by all-atom MD simulation. (c) Transmission electron micrograph (TEM) of JigSAP. Scale bar: 100 nm. (d) Photograph of JigSAP after 48-h incubation at 37 $^{\circ}\text{C}$. The arrow points to the hydrogel. Scale bar: 5 mm. (e) Experimental design: Seven days after distal middle cerebral artery occlusion (dMCAO), motor coordination is assessed by a foot-fault test (FFT), then (f–o) peptide mixtures (PBS as a control, JigSAP only, VEGF-JigSAP only, VEGF + JigSAP, and VEGF-JigSAP + JigSAP) are injected into the injured area. Seven days after peptide injection, the mice are retested for motor coordination and then perfusion-fixed. (f–j) laminin (green) and EdU (magenta) images at the border of the injured core and the penumbra. (k–o) High magnification images of laminin (green), EdU (magenta), and DAPI (blue) at the penumbra.²² Reproduced from reference 22 with permission from Nature Publishing Group, copyright 2021.

in the injured area when VEGF-JigSAP and JigSAP peptides are used (Fig. 4j and o). These results imply the promotion of angiogenesis in the injured area by incorporation and release of VEGF. The incorporation and releasing properties of JigSAP demonstrate wide applicability to the controlled sustained release of various full-length growth factors, which should be useful as artificial scaffolds for tissue regeneration.

Redox-responsive supramolecular peptide fibres for kinetics-controlled cargo release

In applications of stimuli-responsive peptides, the control of the response rate is an important issue to coincide with the target biological events.^{48–54} Redox-active, gel-forming peptides with a methionine (Met) residue in different positions can be used to control the kinetics of the stimulus-responsive gel–sol transition (Fig. 5a and b).⁵⁵ Met is a redox-active amino acid that is oxidised by reactive oxygen species such as H₂O₂, producing methionine sulfoxide (MetO).⁵⁵ JigSAP-IMI and JigSAP-MII and their oxidised forms (JigSAP-IMI-Ox and JigSAP-MII-Ox, respectively), despite this single-point mutation, show contrasting macroscopic properties. Namely, JigSAP-IMI-Ox and JigSAP-MII-Ox remain dispersed in solution under a physiological condition (4 mM HEPES, pH 7.4, DMEM containing 1.0 wt% peptide concentration), whereas JigSAP-IMI and JigSAP-MII form hydrogels under the same

condition. The phase transition from gel to sol is useful for drug and cargo release. Upon addition of 30% H₂O₂ aq. to the top of the hydrogels composed of fluorescent Cy3-labeled JigSAP-IMI and JigSAP-MII ([Cy3-labeled JigSAP-IMI]/[JigSAP-IMI] = 1/99, 1 wt%), the fluorescence intensity derived from the Cy3-labeled-JigSAP-IMI gradually increased (Fig. 5c). The fluorescence change in Cy3-labeled-JigSAP-IMI reached a plateau after >90 min of incubation, consistent with the gel-to-sol transition of the JigSAP-IMI hydrogel (Fig. 5e, black circles). Importantly, Cy3-labeled JigSAP-MII was also released from the JigSAP-MII hydrogel ([Cy3-labeled JigSAP-MII]/[JigSAP-MII] = 1/99, 1 wt%) (Fig. 5d), but the release kinetic was significantly faster than that of Cy3-labeled JigSAP-IMI (Fig. 5e, blue squares). This result demonstrates that the kinetics of cargo release from supramolecular hydrogels can be controlled by adjusting the position of redox-reactive amino acid residues.

Highly stable phospholipid membrane nanosheets with self-assembling peptides enabling extended blood circulation

Cell membranes composed of phospholipid bilayers are important components that regulate vital cellular activities such as substance transportation, signal transduction, and cell adhesion by forming the interface between the intracellular and extracellular environments.

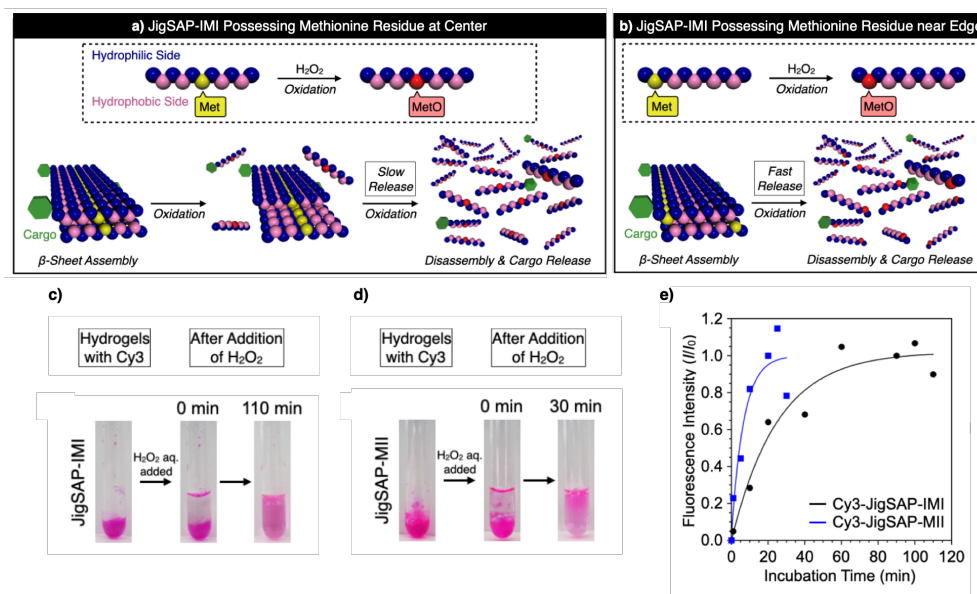


Fig. 5 Schematic illustration of the supramolecular fibre formation of (a) JigSAP-IMI and (b) JigSAP-MII by the β -sheet assembly and subsequent oxidation-triggered disassembly and cargo release. (a) JigSAP-IMI possessing a methionine residue at the center shows relatively slow disassembly and release upon oxidation. (b) JigSAP-MII possessing a methionine residue near an edge shows faster oxidation-triggered disassembly and release. Photographs of (c) JigSAP-IMI hydrogel containing Cy3-JigSAP-IMI and (d) JigSAP-MII hydrogel containing Cy3-JigSAP-MII and their time-course observations after the addition of H₂O₂ aq. to the top of the hydrogels. (e) Time-course changes of fluorescence intensities of Cy3-JigSAP-IMI (black circles) and Cy3-JigSAP-MII (blue squares) released into the solution phases from the JigSAP-IMI and JigSAP-MII hydrogels, respectively, after the addition of 30% H₂O₂ aq. The fluorescence intensities (*I*) of Cy3 are normalized by the intensities (*I*₀) measured after the fully dissolved samples.²³ Reproduced from reference 23 with permission from Wiley, copyright 2023.

To mimic such functions of the cellular membrane, phospholipid assemblies, as represented by liposomes and micelles, have long been used as versatile biomaterials.^{56,57} Of them, phospholipid nanosheets, sometimes called bicelles, have recently attracted particular attention as a material motif to design a drug delivery carrier, because disk-shaped carriers tend to show longer circulation times⁵⁸ and stronger adhesion to microvascular networks^{59,60} than spherical carriers. However, bicelles composed of mixtures of surfactants and phospholipids are essentially unstable and tend to undergo phase transitions and morphological changes upon alteration of the external environment. Phospholipid nanosheets that can be used for blood administration are prepared by designing surfactants incorporating self-assembling peptides.⁶¹ Cholic acid is known to localize at the edge of the phospholipid membrane to afford phospholipid nanosheets.⁶² A cholic acid derivative conjugating a metal-binding peptide sequence PHGGGPHGG (Chol-MBP; Fig. 6a) is designed as a surfactant. DPPC/Chol-MBP nanosheets are formed by mixing dipalmitoylphosphatidylcholine (DPPC) with Chol-MBP ([DPPC]/[Chol-MBP] = 5/1, 5.0 wt% in total). PHGGG is a naturally occurring Cu²⁺-binding motif because of the metal-coordination ability of the imidazole group of the histidine residue.⁶³ Since Chol-MBP can bind to two Cu²⁺ ions, Chol-MBP can self-assemble at the edge of the DPPC/Chol-MBP membrane to inhibit its dissociation (Fig. 6b), thereby enhancing the stability of the phospholipid nanosheets against dilution. When the DPPC/Chol-MBP nanosheets dispersion is diluted to 0.2 wt%, spherical aggregates of less than 100 nm in diameter are observed on TEM (Fig. 6c). Meanwhile, the nanosheet structure is maintained upon the same dilution process after the addition of 2.0 equivalents of Cu²⁺ ions (Fig. 6d), indicating that Cu²⁺-mediated crosslinking of Chol-MBP significantly improves the stability of DPPC/Chol-MBP nanosheets in the diluted condition. The structurally stable DPPC/Chol-MBP/Cu nanosheets can be used to investigate the dependence of the phospholipid assembling morphologies on the blood circulation profiles. Fluorescent Cy5-labeled DPPC vesicles and DPPC/Chol-MBP/Cu nanosheets filtered through a membrane with 200-nm pores are administered to mice via the tail vein (^{FL}DPPC vesicle and ^{FL}DPPC/Chol-MBP/Cu nanosheet, respectively, total content: 5.0 wt% before the injection). Observation of the blood circulation profile by confocal laser scanning microscopy of the earlobe of the mice (IV-CLSM) showed contrasting circulation properties of the vesicles and nanosheets. The ^{FL}DPPC vesicles were aggregated and clogged (Fig. 6f), whereas ^{FL}DPPC/Chol-MBP/Cu nanosheets were homogeneously dispersed in the blood vessels (Fig. 6g). The self-assembling approach of Chol-MBP is thus advantageous for stabilizing the bicelle morphology to enable prolonged circulation in the blood vessel relative to the spherical vesicles, demonstrating a suitable carrier for the whole body by blood administration.

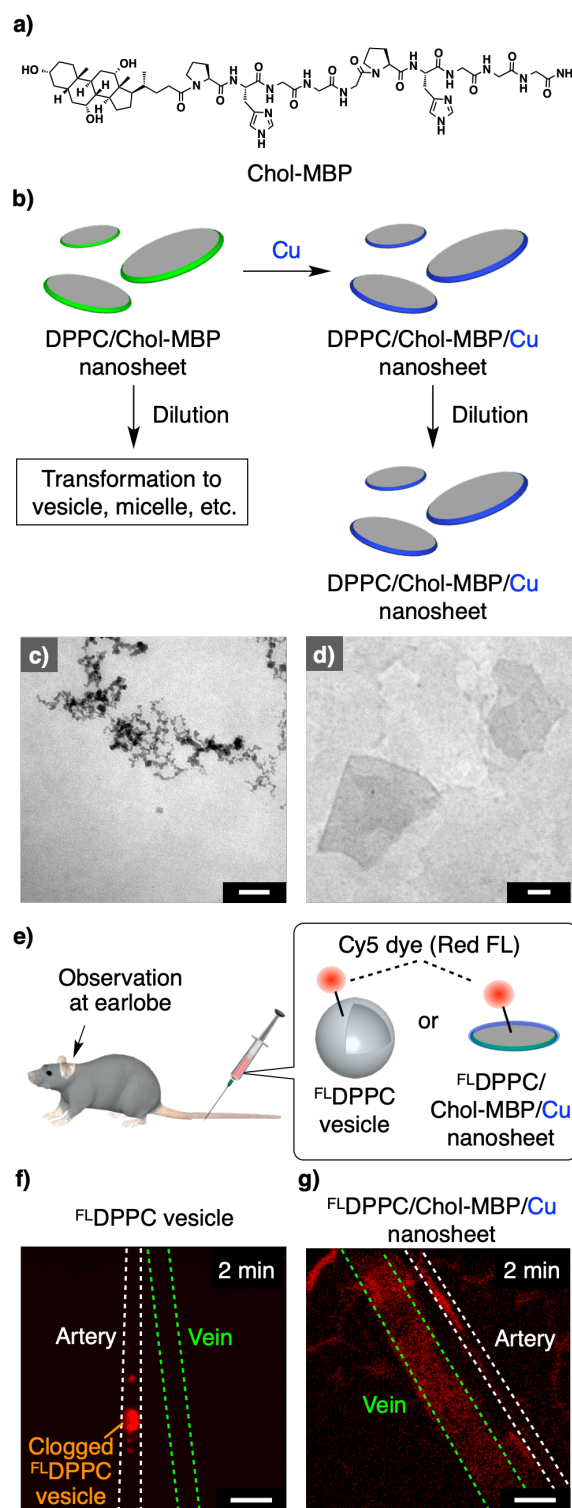


Fig. 6 (a) Molecular structures of Chol-MBP. (b) Schematic illustration of the preparation of DPPC/Chol-MBP nanosheets and subsequent Cu²⁺-mediated metal coordination at Chol-MBP affording crosslinked DPPC/Chol-MBP/Cu nanosheets. After the crosslinking, the disk structure of DPPC/Chol-MBP/Cu nanosheets becomes stable against diluted and serum protein-containing conditions. TEM images of the mixtures of DPPC and Chol-MBP (c)

without and (d) with 2.0 equivalents of Cu^{2+} . Scale bars: 100 nm. (e) Diagram showing the *in vivo* delivery of $^{\text{FL}}$ DPPC and $^{\text{FL}}$ DPPC/Chol-MBP/Cu nanosheets. IV-CLSM images of blood vessels in a mouse earlobe 2 min after the injection of (f) $^{\text{FL}}$ DPPC vesicles and (g) $^{\text{FL}}$ DPPC/Chol-MBP/Cu nanosheets. Scale bars: 100 μm .⁶¹ Reproduced from reference 61 with permission from the Royal Society of Chemistry, copyright 2022.

Liposomes undergoing endocytosis-like fission by a membrane-expanding molecular machine for *in vivo* delivery of viruses

Among biological membrane transport systems, endocytosis^{64–69} is a universal cellular process in which a variety of extracellular substances, ranging from small biomolecules to micrometer-size substances that interact with the cell surface, are taken up via outside-in vesicle fission. Endocytic vesicle fission is closely associated with viral infection,^{64,65} signal transduction in neurons,^{66,67} and phagocytosis associated with immune responses.^{68,69} In cellular endocytosis, biomolecular machines hybridized with cellular membranes enable the uptake of external substances in conjunction with outside-in vesicle fission. However, a molecular approach that enables endocytosis-like transport where membrane deformation is synchronized with substance transport remains critically unexplored.^{70–73} Artificial endocytosis can be induced by using an amphiphilic molecular machine (AzoMEx) containing a diazocine core (Fig. 7a–d),⁷⁴ which undergoes an opening-closing motion by photoisomerization⁷⁵ to change the distance between two cationic NMe_3^+ moieties. Interestingly, the light-triggered mechanical motion of AzoMEx embedded in a 1,2-dioleoyl-*sn*-glycero-3-phosphocholine (DOPC)-based giant unilamellar vesicle can expand the liposomal membrane and induce outside-in fission ($\text{GUV}_{\text{DOPC}/\text{AzoMEx}}$; $[\text{DOPC}] = 180 \mu\text{M}$, $[\text{AzoMEx}] = 20 \mu\text{M}$). This endocytosis-like membrane deformation of $\text{GUV}_{\text{DOPC}/\text{AzoMEx}}$ is useful for the efficient incorporation of large biomacromolecules into the liposomes. $\text{GUV}_{\text{DOPC}/\text{AzoMEx}}$ can interact with the 1- μm -long anionic M13 phage virus due to the cationic property of AzoMEx. When the outside-in fission of $\text{GUV}_{\text{DOPC}/\text{AzoMEx}}$ is induced in the presence of M13 phage virus (22.6×10^{11} virions/mL), M13 phages, as well as AzoMEx, accumulate in the deforming membrane area, and in turn, M13 phages are efficiently incorporated into $\text{GUV}_{\text{DOPC}/\text{AzoMEx}}$ (Fig. 7e–j). M13 phages encapsulated into $\text{GUV}_{\text{DOPC}/\text{AzoMEx}}$ were transiently protected from external environments, keeping their infectivity. A fluorescent Cy5-labelled M13 phage (M13 phage_{Cy5}) encapsulated in $\text{GUV}_{\text{DOPC}/\text{AzoMEx}}$ whose surface is coated with a block polymer composed of poly(aspartic acid) and poly(ethylene glycol) ($\text{GUV}_{\text{DOPC}/\text{AzoMEx}}\text{-pAsp}$) is administered to mice via the tail vein, and M13 phage_{Cy5} shows higher stability in blood (Fig. 7k and l) than bare M13 phage_{Cy5} (Fig. 7l and m), as observed by IV-CLSM of the earlobe vessels. After blood administration of M13 phages encapsulated in

$\text{GUV}_{\text{DOPC}/\text{AzoMEx}}\text{-pAsp}$, the liver, kidney, spleen, lung, heart, and brain were extracted. Importantly, even after distribution to the respective organs through the blood circulation, the infectivity of the M13 phages was retained (spleen: $[25.6 \pm 13.2] \times 10^9$ virions/mg, Fig. 7n; liver: $[18.3 \pm 3.2] \times 10^9$ virions/mg, Fig. 7o; kidney: $[1.3 \pm 0.6] \times 10^9$ virions/mg, Fig. 7p; heart: $[1.1 \pm 0.5] \times 10^9$ virions/mg, Fig. 7q; lung: $[0.5 \pm 0.3] \times 10^9$ virions/mg, Fig. 7r; and brain: $[0.2 \pm 0.1] \times 10^9$ virions/mg, Fig. 7s). The membrane-expanding molecular machine AzoMEx functionalizes GUV for endocytosis-like fission, which is useful for encapsulation and delivery of biomacromolecules. M13 phages are commonly used in phage display, with the use of affinity selection to identify peptides that bind to target molecules. Therefore, the AzoMEx-GUV technology to encapsulate M13 phages for protection from immune cells in the blood could be applied to an *in vivo* phage display method for the selection of peptides that bind to ligands in living bodies.^{76,77}

Conclusions

A bio-interface is a field of contact between molecules, cells, and tissues for interactions. The interactions at the bio-interfaces are major triggers regulating a wide variety of physiological actions such as adhesion, signaling, and substance transportation. Therefore, understanding the molecular mechanisms underlying that contact is one of the central subjects in biological science. For bioengineering, regulation of the bio-interfaces is one effective approach, and chemistry can contribute to the development of bottom-up methodologies for bio-interface manipulation. In this Feature Article, our recent studies about the development of supramolecular materials mimicking the contact events at the bio-interfaces were highlighted. The ECM is a fundamental tissue at the cellular interface constructed by networks of fibrous proteins, which regulates a variety of cellular activities. Reconstruction of the ECM has been demonstrated by self-assembling peptides. Conjugation of the peptides with proteins allows for displaying N-cadherin and VEGF onto the supramolecular nanofibres. By combining the dynamic properties of the self-assembling peptides with displaying N-cadherin and sustained-releasing VEGF, the protein-peptide conjugated materials enable neuronal migration and regeneration of injured neural tissue. The dynamic properties of the self-assembling peptides can be effectively controlled by point mutations such as amino acid replacement in the main chain and structural modification by redox in the side chain. The phospholipid bilayer is the main component of the cell membrane. The morphology and deformation of the phospholipid bilayer relate directly to the dynamic interfacial functions. Stabilization of the phospholipid nanosheet structure has been demonstrated by synthetic surfactant bearing metal-chelating, self-assembling peptides. The stabilized bicelle is functional for extended blood circulation. By using photo-responsive synthetic surfactant showing a mechanical opening/closing motion, endocytosis-like outside-in membrane deformation is triggered. The outside-in deformation allows for efficient encapsulation of micrometer-size substances such as phage viruses into the liposomes and protects them from external environments. The encapsulated viruses can be delivered to multiple organs in a living body via blood administration.

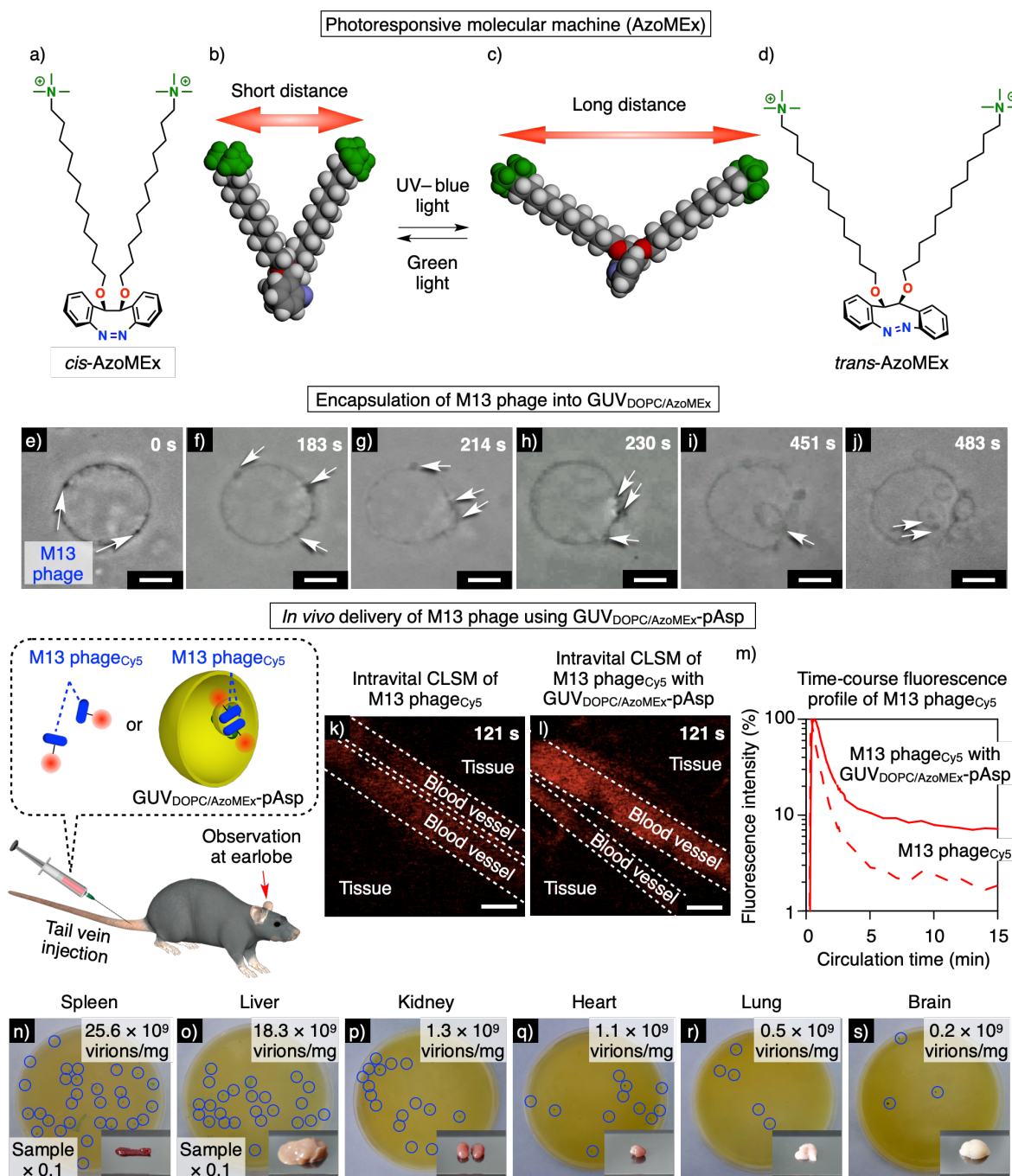


Fig. 7 Molecular structures of a photoresponsive molecular machine, AzoMEx, in its (a) *cis*-form and (d) *trans*-form consisting of a diazocine core with appending $-NMe_3^+$ groups and an alkoxide spacer. (b, c) Schematic images of the mechanical motion of AzoMEx during *cis*-to-*trans* photoisomerization, which changes the distance between the $-NMe_3^+$ groups on UV-blue (for *cis*-to-*trans* isomerization) and green (for *trans*-to-*cis* isomerization) light irradiation. Phase-contrast microscopic observations of the uptake of M13 phages into GUV_{DOPC/AzoMEx} under 370-nm light irradiation. Snapshots are taken at (e) 0 s, (f) 183 s, (g) 214 s, (h) 230 s, (i) 451 s, and (j) 483 s after starting the light irradiation. Scale bars: 5 μ m. White arrows indicate M13 phages. Intravital CLSM images of blood vessels in a mouse earlobe 121 s after tail vein injection of (k) M13 phages_{Cy5} or (l) GUV_{DOPC/AzoMEx}-pAsp encapsulating M13 phages_{Cy5}. Scale bars: 100 μ m. (m) Time-course profiles over 15 min of the fluorescence intensity in the blood vessels of unencapsulated M13 phages_{Cy5} (dashed line) and M13 phages_{Cy5} encapsulated into GUV_{DOPC/AzoMEx}-pAsp (solid line). Plaque assays of homogenized samples of (n) spleen, (o) liver, (p) kidney, (q) heart, (r) lung, and (s) brain 15 min after injection of 100 μ L of GUV_{DOPC/AzoMEx}-pAsp encapsulating M13 phages. The samples of spleen and liver are diluted 10-fold before the plaque assay. Insets: photographs of the corresponding organs. Representative spots of M13 phage-infected *E. coli* in (o–t) are indicated by blue circles.⁷⁴ Reproduced from reference 74 with permission from the American Chemical Society, copyright 2023.

These supramolecular approaches to mimicking and controlling bio-interfaces present powerful ways to develop unprecedented regenerative medicines and drug delivery systems. The materials science needed to reconstruct biomimetic interfaces with a dynamic nature is still in its infancy and is expected to make significant progress in the future toward biomedical applications.

Author Contributions

Both authors have discussed the organization and presentation of the contents and participated in the writing and editing of the Feature Article.

Conflicts of Interest

There are no conflicts to declare.

Acknowledgements

This work was supported by a Grant-in-Aid for Transformative Research Areas (B) JP21H05096 (TM), a Grant-in-Aid for Scientific Research (C) JP23K04927 (NU), Japan Science Technology Agency CREST JPMJCR19S4 (TM), FOREST JPMJFR2122 (TM), Asahi Glass Foundation (NU, TM), Moritani Scholarship Foundation (NU) and Takeda Science Foundation (TM). We thank Prof. Itsuki Ajioka, Prof. Yasutaka Anraku, Prof. Naoko Kaneko, and Prof. Kazunobu Sawamoto for *in vivo* experiments, Prof. Go Watanabe for MD simulation, Prof. Hirotsugu Hiramatsu for IR analysis, Dr. Takashi Kajitani for X-ray analysis, and Prof. Teruhiko Matsubara and Prof. Toshinori Sato for experiments using bacteriophages.

Notes and references

- R. O. Hynes, *Science* 2009, **326**, 1216–1219.
- K. H. Vining and D. J. Mooney, *Nat. Rev. Mol. Cell Biol.* 2017, **18**, 728–742.
- A. Gallet, L. Ruel, L. Staccini-Lavenant and P. P. Théron, *Development* 2006, **133**, 407–418.
- A. Callejo, C. Torroja, L. Quijada and I. Guerrero, *Development* 2006, **133**, 471–483.
- I. Canton and G. Battaglia, *Chem. Soc. Rev.* 2012, **41**, 2718–2739.
- S. Arandjelovic and K. S. Ravichandran, *Nat. Immunol.* 2015, **16**, 907–917.
- W. Shin, L. Ge, G. Arpino, S. A. Villarreal, E. Hamid, H. Liu, W.-D. Zhao, P. J. Wen, H.-C. Chiang and L.-G. Wu, *Cell* 2018, **173**, 934–945.
- A. Sorushanova, L. M. Delgado, Z. Wu, N. Shologu, A. Kshirsagar, R. Raghunath, A. M. Mullen, Y. Bayon, A. Pandit, M. Raghunath and D. I. Zeugolis, *Adv. Mater.* 2019, **31**, 1801651.
- W. Zheng, W. Zhang and X. Jiang, *Adv. Eng. Mat.* 2010, **12**, B451–B466.
- J. A. Kluge, O. Rabotyagova, G. G. Leisk and D. L. Kaplan, *Trends Biotechnol.* 2008, **26**, 244–251.
- A. Rising, M. Widhe, J. Johansson and M. Hedhammar, *Cell. Mol. Life Sci.* 2011, **68**, 169–184.
- J. D. Hartgerink, E. Beniash and S. I. Stupp, *Science* 2001, **294**, 1684–1688.
- Z. Álvarez, A. N. Kolberg-Edelbrock, I. R. Sasselli, J. A. Ortega, R. Qiu, Z. Syrgiannis, P. A. Mirau, F. Cheng, S. M. Chin, S. Weigand, E. Kiskinis and S. I. Stupp, *Science* 2021, **374**, 848–856.
- G. A. Silva, C. Czeisler, K. L. Niece, E. Beniash, D. A. Harrington, J. A. Kessler and S. I. Stupp, *Science* 2004, **303**, 1352–1355.
- X. Yan, P. Zhu and J. Li, *Chem. Soc. Rev.* 2010, **39**, 1877–1890.
- S. Fleming and R. V. Ulijn, *Chem. Soc. Rev.* 2014, **43**, 8150–8177.
- T. L. Lopez-Silva, D. G. Leach, A. Azares, I. C. Li, D. G. Woodside and J. D. Hartgerink, *Biomaterials* 2020, **231**, 119667.
- L. A. Haines, K. Rajagopal, B. Ozbas, D. A. Salick, D. J. Pochan and J. P. Schneider, *J. Am. Chem. Soc.* 2005, **127**, 17025–17029.
- H. Yokoi, T. Kinoshita and S. Zhang, *Proc. Natl. Acad. Sci. U. S. A.* 2005, **102**, 8414–8419.
- A. Ishida, G. Watanabe, M. Oshikawa, I. Ajioka and T. Muraoka, *Chem. Eur. J.* 2019, **25**, 13523–13530.
- Y. Ohno, C. Nakajima, I. Ajioka, T. Muraoka, A. Yaguchi, T. Fujioka, S. Akimoto, M. Matsuo, A. Lotfy, S. Nakamura, V. Herranz-Pérez, J. M. García-Verdugo, N. Matsukawa, N. Kaneko and K. Sawamoto, *Biomaterials* 2023, **294**, 122003.
- A. Yaguchi, M. Oshikawa, G. Watanabe, H. Hiramatsu, N. Uchida, C. Hara, N. Kaneko, K. Sawamoto, T. Muraoka and I. Ajioka, *Nat. Commun.* 2021, **12**, 6623.
- Y. Hara, A. Yaguchi, H. Hiramatsu and T. Muraoka, *ChemBioChem* 2023, DOI: 10.1002/cbic.202200798.
- O. J. G. M. Goor, S. I. S. Hendrikse, P. Y. W. Dankers and E. W. Meijer, *Chem. Soc. Rev.* 2017, **46**, 6621–6637.
- S. Zhang, M. Xing and B. Li, *Int. J. Mol. Sci.* 2018, **19**, 1641.
- W. A. Abbas, M. E. Ibrahim, M. El-Naggar, W. A. Abass, I. H. Abdullah, B. I. Awad and N. K. Allam, *ACS Biomater. Sci. Eng.* 2020, **6**, 6490–6509.
- J. Morstein, R. Z. Hill, A. J. E. Novak, S. Feng, D. D. Norman, P. C. Donthamsetti, J. A. Frank, T. Harayama, B. M. Williams, A. L. Parrill, G. J. Tigyi, H. Riezman, E. Y. Isacoff, D. M. Bautista and D. Trauner, *Nat. Chem. Biol.* 2019, **15**, 623–631.
- A. A. Vorobieva, P. White, B. Liang, J. E. Horne, A. K. Bera, C. M. Chow, S. Gerben, S. Marx, A. Kang, A. Q. Stiving, S. R. Harvey, D. C. Marx, G. N. Khan, K. G. Fleming, V. H. Wysocki, D. J. Brockwell, L. K. Tamm, S. E. Radford and D. Baker, *Science* 2021, **371**, eabc8182.
- H. Wichterle, J. M. García-Verdugo and A. Alvarez-Buylla, *Neuron* 1997, **18**, 779–791.
- C. Lois, J. M. García-Verdugo and A. Alvarez-Buylla, *Science* 1996, **271**, 978–981.
- P. Thored, A. Arvidsson, E. Cacci, H. Ahlenius, T. Kallur, V. Darsalia, C. T. Ekdahl, Z. Kokaia and O. Lindvall, *Stem Cell* 2006, **24**, 739–747.
- E. Llorens-Bobadilla, S. Zhao, A. Baser, G. Saiz-Castro, K. Zwadlo and A. Martin-Villalba, *Cell Stem Cell* 2015, **17**, 329–340.
- N. Kaneko, V. Herranz-Pérez, T. Otsuka, H. Sano, N. Ohno, T. Omata, H. B. Nguyen, T. Q. Thai, A. Nambu, Y. Kawaguchi, J. M. García-Verdugo and K. Sawamoto, *Sci. Adv.* 2018, **4**, eaav0618.
- N. S. Roy, C. Cleren, S. K. Singh, L. Yang, M. F. Beal and S. A. Goldman, *Nat. Med.* 2006, **12**, 1259–1268.
- T. Yamashita, H. Kawai, F. Tian, Y. Ohta and K. Abe, *Cell Transplant.* 2011, **20**, 883–892.
- K. Ohnishi, K. Semi, T. Yamamoto, M. Shimizu, A. Tanaka, K. Mitsunaga, K. Okita, K. Osafune, Y. Arioka, T. Maeda, H.

- Soejima, H. Moriwaki, S. Yamanaka, K. Woltjen and Y. Yamada, *Cell* 2014, **156**, 663–677.
- 37 M. I. Echeverria Molina, K. G. Malollari and K. Komvopoulos, *Front. Bioeng. Biotechnol.* 2021, **9**, 1–29.
- 38 T. Santos, C. Boto, C.M. Saraiva, L. Bernardino and L. Ferreira, *Trends Biotechnol.* 2016, **34**, 437–439.
- 39 A. Cembran, K. F. Bruggeman, R. J. Williams, C. L. Parish and D. R. Nisbet, *iScience* 2020, **23**, 100788.
- 40 D. Carradori, J. Eyer, P. Saulnier, V. Pr eat and A. des Rieux, *Biomaterials* 2017, **123**, 77–91.
- 41 N. Kaneko, M. Sawada and K. Sawamoto, *J. Neurochem.* 2017, **141**, 835–847.
- 42 M. M. Martino, P. S. Briquez, E. G uc, F. Tortelli, W. W. Kilarski, S. Metzger, J. J. Rice, G. A. Kuhn, R. M uller, M. A. Swartz and J. A. Hubbell, *Science* 2014, **343**, 885–888.
- 43 M. Mochizuki, E. G uc, A. J. Park, Z. Julier, P. S. Briquez, G. A. Kuhn, R. M uller, M. A. Swartz, J. A. Hubbell and M. M. Martino, *Nat. Biomed. Eng.* 2020, **4**, 463–475.
- 44 Y. Sun, K. Jin, L. Xie, J. Childs, X. O. Mao, A. Logvinova and D. A. Greenberg, *J. Clin. Invest.* 2003, **111**, 1843–1851.
- 45 Y. Wang, K. Jin, X. O. Mao, L. Xie, S. Banwait, H. H. Marti and D. A. Greenberg, *J. Neurosci. Res.* 2007, **85**, 740–747.
- 46 G. Kleiger, R. Grothe, P. Mallick and D. Eisenberg, *Biochemistry* 2002, **41**, 5990–5997.
- 47 W. Liu, E. Crocker, W. Zhang, J. I. Elliott, B. Luy, H. Li, S. Aimoto and S. O. Smith, *Biochemistry* 2005, **44**, 3591–3597.
- 48 Y. Gao, Y. Kuang, Z.-F. Guo, Z. Guo, I. J. Krauss and B. Xu, *J. Am. Chem. Soc.* 2009, **131**, 13576–13577.
- 49 Y. Kumada, N. A. Hammond and S. Zhang, *Soft Matter* 2010, **6**, 5073–5079.
- 50 Q. Xu, C. He, K. Ren, C. Xiao and X. Chen, *Adv. Healthcare Mater.* 2016, **5**, 1979–1990.
- 51 R. Petitdemange, E. Garanger, L. Bataille, K. Bathany, B. Garbay, T. J. Deming and S. Lecommandoux, *Bioconjugate Chem.* 2017, **28**, 1403–1412.
- 52 D. Spitzer, L. L. Rodrigues, D. Stra burger, M. Mezger and P. Besenius, *Angew. Chem. Int. Ed.* 2017, **56**, 15461–15465.
- 53 C. Chen, J. Wang, R. Hao, Z. Wang, Z. Hou, Y. Zhao, C. Zong and H. Xu, *ACS Appl. Bio Mater.* 2018, **1**, 2110–2119.
- 54 J. Shi, G. Fichman and J. P. Schneider, *Angew. Chem. Int. Ed.* 2018, **57**, 11188–11192.
- 55 X. Liang, A. Kaya, Y. Zhang, D. T. Le, D. Hua and V. N. Gladyshev, *BMC Biochem.* 2012, **13**, 21.
- 56 A. Sharma and U. S. Sharma, *Int. J. Pharm.* 1997, **154**, 123–140.
- 57 G. Bozzuto and A. Molinari, *Int. J. Nanomed.* 2015, **10**, 975–999.
- 58 S. Muro, C. Garnacho, J. A. Champion, J. Leferovich, C. Gajewski, E. H. Schuchman, S. Mitragotri and V. R. Muzykantov, *Mol. Ther.* 2008, **16**, 1450–1458.
- 59 N. Doshi, B. Prabhakarandian, A. Rea-Ramsey, K. Pant, S. Sundaram and S. Mitragotri, *J. Control. Release.* 2010, **146**, 196–200.
- 60 G. Adriani, M. D. de Tullio, M. Ferrari, F. Hussain, G. Pascazio, X. Liu and P. Decuzzi, *Biomaterials* 2012, **33**, 5504–5513.
- 61 Y. Takagi, N. Uchida, Y. Anraku and T. Muraoka, *Chem. Commun.* 2022, **58**, 5164–5167.
- 62 K. S. Mineev, K. D. Nadezhdin, S. A. Goncharuk and A. S. Arseniev, *Langmuir* 2016, **32**, 6624–6637.
- 63 S. Ghosh and S. Verma, *Tetrahedron Lett.* 2007, **48**, 2189–2192.
- 64 D. S. Dimitrov, *Cell* 2003, **115**, 652–653.
- 65 S. Igonet and F. A. Rey, *Cell* 2012, **151**, 1634–1634.e1.
- 66 S. Watanabe, B. R. Rost, M. Camacho-P erez, M. W. Davis, B. S ohl-Kielczynski, C. Rosenmund and E. M. Jorgensen, *Nature* 2013, **504**, 242–247.
- 67 S. O. Rizzoli and W. J. Betz, *Science* 2004, **303**, 2037–2039.
- 68 C. Settembre, C. D. Malta, V. A. Polito, M. G. Arencibia, F. Vetrini, S. Erdin, S. U. Erdin, T. Huynh, D. Medina, P. Colella, M. Sardiello, D. C. Rubinsztein and A. Ballabio, *Science* 2011, **332**, 1429–1433.
- 69 T. Yeung, M. Terebiznik, L. Yu, J. Silvius, W. M. Abidi, M. Philips, T. Levine, A. Kapus and S. Grinstein, *Science* 2006, **313**, 347–351.
- 70 R. Lipowsky, *Phys. A* 1993, **194**, 114–127.
- 71 T. Hamada, Y. T. Sato, K. Yoshikawa, T. Nagasaki, *Langmuir* 2005, **21**, 7626–7628.
- 72 C. Pernpeintner, J. A. Frank, P. Urban, C. R. Roeske, S. D. Pritzl, D. Trauner, T. Lohm uller, *Langmuir* 2017, **33**, 4083–4089.
- 73 T. Baumgart, S. T. Hess, W. W. Webb, *Nature* 2003, **425**, 821–824.
- 74 N. Uchida, Y. Ryu, Y. Takagi, K. Yoshizawa, K. Suzuki, Y. Anraku, I. Ajioka, N. Shimokawa, M. Takagi, N. Hoshino, T. Akutagawa, T. Matsubara, T. Sato, Y. Higuchi, H. Ito, M. Morita and T. Muraoka, *J. Am. Chem. Soc.* 2013, DOI: 10.1021/jacs.2c12348.
- 75 R. Siewertsen, H. Neumann, B. Buchheim-Stehn, R. Herges, C. N ather, F. Renth and F. Temps, *J. Am. Chem. Soc.* 2009, **131**, 15594–15595.
- 76 J. W. Kehoe and B. K. Kay, *Chem. Rev.* 2005, **105**, 4056–4072.
- 77 H. H. Gustafson, A. Olshefsky, M. Sylvestre, D. L. Sellers and S. H. Pun, *Adv. Drug Delivery Rev.* 2018, **130**, 39–49.